Is $[ReCl_4(CN)_2]^{2-}$ a good Building Block for Single Molecule Magnets? A Theoretical Investigation.

Christoph van Wüllen[⋆,†] and Eva M. V. Keßler[†]

[⋆] ORCID: 0000-0001-7632-3437, eMail: vanwullen@chemie.uni-kl.de

[†] Fachbereich Chemie and Forschungszentrum OPTIMAS,

Technische Universität Kaiserslautern,

67663 Kaiserslautern, Germany.

January 5, 2022

Abstract

Building blocks containing 5*d* spin centres are promising for constructing single molecule magnets due to their large spin-orbit interaction, but experimental and computational results obtained so far indicate that this might not be the case for Re^{IV} centres in an octahedral environment. Density functional results obtained in this work for $[ReCl_4(CN)_2]^{2-}$ and trinuclear complexes formed by attaching Mn^{II} centres to the cyano ligands indicate that zero field splitting in such complexes exhibits large rhombicity (which leads to fast relaxation of the magnetisation) even if there are only small distortions from an ideal geometry with a four-fold symmetry axis. This is already apparent if second-order spin-orbit perturbation theory is applied but even more pronounced if higher-order spin-orbit effects are included as well, as demonstrated by wave function based calculations. Computational results are cast into a ligand field model and these simulations show that especially a distortion which is not along the C_4/C_2 axes has a large effect on the rhombicity. Quantum simulations on these complexes are difficult because the zero field splitting strongly depends on the energetic position of the low-lying doublets from the t_{2g}^3 configuration.

1 Introduction

In single molecule magnets (SMMs), magnetic properties of a sample arise from individual molecules, which may be isolated from each other. This makes it possible at least in principle, to store (and process) information using single molecules,[1,2] and this would be a large step towards further miniaturisation in information technology. Of course, there are major technological problems such as controlled positioning and addressing of such single molecules, but a fundamental question remains, namely how long can a molecule keep the information contained in its magnetic state, thus

resisting thermal and magnetic fluctuations that will ultimately lead to the loss of information (magnetisation). There are several mechanisms that lead to demagnetisation,[3] from this it follows that in order to keep its magnetisation, a molecule should have a ground state spin multiplet with a sufficiently large spin S, which has a uniaxial and easy-axis type zero field splitting (ZFS) (D large and negative and $E \approx 0$, with D and E the usual effective ZFS parameters of the ground state multiplet). A large spin together with almost zero rhombicity ($E \approx 0$) is needed to suppress quantum tunnelling, while the energetic width of the multiplet ($\sim DS^2$) is a limit to the (apparent) activation energy for thermally activated demagnetisation processes. Finally, it is necessary that the ground state multiplet is energetically well separated from excited spin states, such that they do not contribute significantly to demagnetisation pathways. For systems with very large (first-order) zero field splitting the requirements are essentially the same but often cast into a different language, namely that one should have an energetically well-separated Kramers doublet ground state with a large axial and vanishing transversal g values. Note that it is not optimal to have a ground state with a *very* large spin, since this leads to strong long-range interactions *between* the molecules which may speed up demagnetisation in a real sample.

In transition metal complexes, the dominant microscopic origin of zero field splitting is spin-orbit interaction, which strongly grows with the nuclear charge of the spin centres involved. This suggests that large zero field splitting can be expected if $5d$ metals and/or lanthanides are involved. Lanthanides are a special case since ZFS here is limited by the ligand field rather than by the spin-orbit interaction, and the major obstacle in using them as ,,building blocks" for SMMs it that exchange coupling between lanthanides is rather weak unless strongly anionic bridges are used. Using $4d/5d$ metal centres as SMM building blocks has been discussed intensively (see Ref.[4] for a review). Two different Re^{IV} building blocks have been investigated by the Long group, namely $[Re^{IV}(CN)_7]^{3-}$ [5,6] and *trans*-$[Re^{IV}Cl_4(CN)_2]^{2-}$ [7,8]. The former one has large (first-order) spin-orbit splitting leading to a well-separated anisotropic Kramers doublet ground state. This complex shows large transversal g values[5], and coordinates $3d$ centres such that a non-axial geometry[6] results. Although slow magnetic relaxation with an effective barrier height of 17 cm^{-1} was observed when four Ni^{II} centres were attached,[6] the inherent deviation from uniaxiality could be a problem. The *trans*-$[ReCl_4(CN)_2]^{2-}$ anion (**1a**) with a Re^{IV} centre in an octahedral environment (t_{2g}^3 configuration with three unpaired electrons and a $S = 3/2$ ground state) seems attractive since it can coordinate to two further metal centres forming Re-CN-M linkages that result in an overall axial geometry, and a local C_4 axis should lead to small rhombicity. This building block is orbitally non-degenerate and has second-order zero field splitting. An analysis of the temperature-dependent magnetic susceptibility (χT) curve for $(NBu_4)_2ReCl_4(CN)_2$ (**1b**) resulted in a zero field splitting with $D = -14.4$ cm^{-1},[7] but further investigation using high-field electron paramagnetic resonance (EPR)[8] resulted in a positive D value ($D = +11$ cm^{-1}) and extremely large rhombicity ($|E| = 3.2$ cm^{-1}). While the sign of D in the latter case does not matter that much since it is not meaningful in the extreme biaxial case where $|E/D| \approx 1/3$, the large rhombicity found for a complex anion close to the ideal D_{4h} symmetry comes unexpectedly: Obviously, small deviations from the ideal symmetry are enough to build up significant rhombicity. The Long group synthesised the trinuclear $Mn^{II}Re^{IV}Mn^{II}$ complex $(MnPy_5)_2ReCl_4(CN)_2$ (**2**) (using the shorthand notation Py_5 for a pentapyridyl ligand, see Scheme **??**), where two Mn^{II} centres were attached

to the two cyano groups of **1a**[8]. For this compound, antiferromagnetic coupling between Re and Mn was found leading to a $S = 7/2$ ground state, and the ZFS parameter determined by EPR spectroscopy were $D = +0.3$ cm^{-1} and $|E| = 0.03$ cm^{-1}, but the authors stress that there were difficulties in analysing the experimental data such that these numbers contain a significant uncertainty. Assuming that the Mn^{II} atoms only negligibly contribute to ZFS, and that the giant spin approximation (also known as strong exchange limit) largely holds, such a small molecular D value would correspond to a rather small single-ion value $D_{Re} = +4.5$ cm^{-1}.

These findings triggered quantum chemical investigations. The zero field splitting was calculated[9] for a series of Re^{IV} complexes (including **1a**) and a the dependence of the calculated D parameter on the nature of the tetragonal distortion (starting from a perfect octahedral environment that produces $D = 0$) was discussed. For example, while $D = +16.2$ cm^{-1} was found for **1a**, this value increases to $+55.6$ cm^{-1} if the cyano ligands are replaced by pyridine,[9] and the Re-CN bond length also had a significant impact. It became furthermore obvious that the calculated D value critically depends on the type of wave function used: while a complete active space self-consistent field (CASSCF) calculation gave $D = -21$ cm^{-1} for **1a**, adding dynamical electron correlation through second-order perturbation theory (CASPT2) produced the final value, $D = +16.2$ cm^{-1}.[9] This was attributed to the fact that dynamical correlation lowers the doublet states arising from the t_{2g}^3 configuration w.r.t to quartet ground state. The same authors also investigated the Re-CN-Mn linkage with density functional (DFT) methods[10] and found a weak antiferromagnetic interaction between Re and Mn, in agreement with what had been found experimentally for magnetic chains built from **1a** and Mn^{II} building blocks[7]. The purpose of this work is to complement such studies by DFT calculations on trinuclear complexes to explore how the rhombicity could possibly be reduced, and to analyse the strong dependence of the ZFS tensor of **1a** w.r.t. variation of the ligand field by ligand field simulations.

2 Materials and Methods

The starting point for the calculation of molecular magnetic properties is the generation of the molecular structures for the compounds being investigated. The structure of **1a** has been directly taken as a cut-out from the published[7] X-ray structure by removing the counter-ions and a solvent molecule. Two additional variants of this structure have been constructed, namely a D_{2h} symmetric one obtained by setting the NC-Re-Cl angles to 90° while keeping all bond lengths at their experimental value, and a D_{4h} variant where additionally the Re-Cl bond length were made equal, setting them to the mean value of the experimental bond lengths. These structures are used to monitor the build-up of rhombicity when going from the D_{4h} structure (where $E = 0$ for symmetry reasons) to the structure experimentally observed. The structure of **1b** has also been obtained from the X-ray structure, the two symmetry-equivalent NBu_4^+ counter-ions have been kept and only the solvent molecule has been deleted. Then, the hydrogen positions have been optimised by DFT calculations using the PBE0 exchange-correlation functional[11], using the def2-TZVP basis set[12] and a quasi-relativistic effective core potential replacing 60 core electrons[13]. The DFT calculations were performed with our local version of the TURBOMOLE program[14–16] using the Berny geometry optimisation algorithm[17] as implemented in the Gaussian-16 program[18]. The

same procedure has been applied to generate the molecular structure of **2**, the X-ray structure has been obtained from Ref. [8] and the hydrogen positions have been optimised while holding the coordinates of the non-hydrogen atoms fixed. Optimising the hydrogen positions in experimental X-ray structures is a standard procedure in our laboratory since the bond lengths involving hydrogen are usually much too short in the X-ray structures.

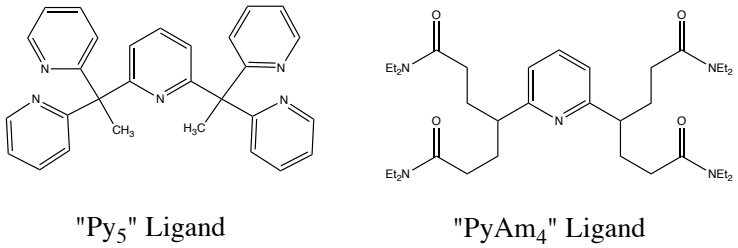

Figure 1: Pentadentate ligands used as ,,end-caps" in trinuclear Mn-Re-Mn complexes. The Py_5 ligand has been used in experimental work (Ref. [8]) while the $PyAm_4$ ligand has only been used in our calculations to support linear Re-CN-Mn linkages.

In the X-ray structure of **2**, the Re-CN-Mn linkage is bent, which perturbs the local C_4 symmetry of the NC-$ReCl_4$-CN unit of the building block **1a**. The same bending is observed when performing a full (unconstrained) DFT geometry optimisation on **2**, and also found experimentally in chain structures where the four remaining coordination sites of the Mn atoms are coordinated by dimethyl formamide (DMF) ligands [8]. Interestingly, a strong influence of this ligand on the amount of bending (zig-zag) in the chain has been observed experimentally for the analogous Fe compounds [19], almost linear (non-bent) chains were obtained when using diethyl amide (DEA) instead of DMF. We have performed DFT optimisations on small models and verified that this should also hold for Re-CN-Mn linkages. Therefore we were tempted to construct a pentadentate ,,end-cap" for the manganese atoms that binds like DEA to the four Mn coordination sites orthogonal to the Re-CN-Mn linkage. The result is the hypothetical $PyAm_4$ ligand (Figure 1) that has four DEA-like ,,arms" connected to a pyridine ring that holds everything together. We have built the $(MnPyAm_4)_2ReCl_4(CN)_2$ molecule (**3a**, **3b**) in the computer and a geometry optimisation resulted, indeed, in linear Re-CN-Mn linkages. We obtained two nearly iso-energetic conformers **3a** and **3b** which differ by the relative orientation of the end-caps: in **3a** the two pyridine rings are coplanar and the optimised structure is close to C_{2h} symmetry, while **3b** approximately has S_4 symmetry and the two pyridine rings are perpendicular to each other (see Figure 2). Note that according to our DFT calculations **3a** and **3b** can interconvert through a rather low barrier by rotating one of the end-caps w.r.t. to the other. The cartesian (XYZ) coordinates of all compounds are documented in the electronic supporting information.

The ZFS **D** tensors and its D and E parameters of all compounds have been calculated using DFT. Relativistic effects (including spin-orbit interaction) have been included via the fourth-order Douglas-Kroll operator [20]. For the spin-orbit interaction, it is especially important to include two-electron relativistic effects, this has been done via the model potential approximation [21] developed

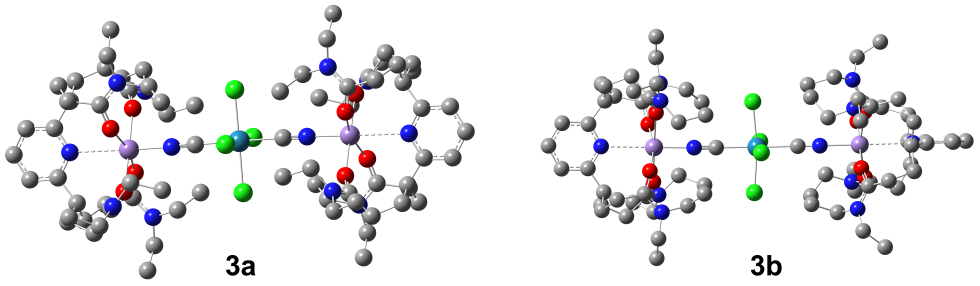

Figure 2: Molecular structure of **3a** (left) and **3b** (right).

by one of us, combined with the suggestion by Neese to scale the exchange part of the DFT effective potential by -2 when calculating spin-orbit matrix elements [22]. The ZFS tensors are calculated by second-order spin-orbit perturbation theory as described in Ref. [23]. It is important to note that DFT cannot be applied in a straightforward way to oligonuclear complexes with antiferromagnetic coupling. Therefore the anisotropic broken symmetry approach [24] has been used to extract single-ion ZFS tensors together with the isotropic exchange coupling constants, and the final molecular ZFS tensors are then calculated by the projection method (see the supporting information for details). In the all-electron Douglas-Kroll calculations, the def2-TZVP basis set [12] was used for all atoms except Re, for which we constructed a new all-electron contracted basis based on an uncontracted basis set by Hirao and Nakajima [25]. The full single-ion ZFS tensors for the Re and Mn centres, and the molecular ZFS tensors obtained by projection, are documented in the supporting information.

In order to identify possible pitfalls of the DFT method, we also calculated the ZFS parameters for mononuclear **1a** and **1b** using a valence-space full configuration interaction method including spin-orbit coupling (CASOCI). The CASOCI program is a new program that includes a module to extract spin Hamiltonian parameters from the ab initio wave function and is described elsewhere [26]. The quasi-relativistic Douglas-Kroll Hamiltonian and the basis sets are the same as in the all-electron DFT calculations except that the matrix elements of the mean-field spin-orbit operator [27] are now used within the Douglas-Kroll transformation. Orbitals are optimised for a weighted average of energy expectation values of Slater determinants, namely the ground configuration t_{2g}^3 with weight 0.8 and an excited configuration $t_{2g}^2 e_g^1$ with a total weight of 0.2 distributed over the six Slater determinants from that configuration. The orbitals are obtained in a scalar relativistic calculation (spin orbit interaction not included in the orbital optimisation step). This technique, namely using a special kind of restricted open shell Hartree-Fock calculation to optimize the orbitals, has been described in more detail in Ref. [28]. The valence full configuration interaction problem is then solved with spin-orbit interaction included.

Ligand field parameters for a system with 3 electrons in 5 *d*-orbitals have been extracted from the CASOCI results. In subsequent ligand field simulations, it has been evaluated how ZFS parameters react to variations of the ligand field, and to a variation of the electron interaction parameter which largely determines the energetic separation between the quartet ground state

and the lowest doublets of the t_{2g}^3 manifold. The ligand field simulations are described in detail in the supporting information. Briefly, the two-electron matrix elements are characterised by a single parameter (namely the Racah parameter B, keeping the ratio C/B fixed). The ligand field is parametrized by parameters for the octahedral field, the σ- and π-components of the tetragonal distortion, and a rhombic and trigonal distortion. Starting from the octahedral case, the π component of the tetragonal distortion removes the degeneracy of the t_{2g} orbitals, while the corresponding σ component does this to the e_g orbitals. The rhombic distortion further removes the degeneracy of d_{xz} and d_{yz}, while a trigonal distortion can be imagined as compressing or expanding the octahedron along one of its C_3 axes. The main reason to perform these ligand field simulations was to understand why the D value for a Re^{IV} is so sensitive to details of the calculation and the ligand field, and why the ZFS of the building block **1a** has such a large rhombicity although its (experimental) molecular structure is close to the idealised D_{4h} one, for which there would be no rhombicity for symmetry reasons.

3 Results and discussion

3.1 Density functional results

We start by presenting the ZFS parameters calculated for all compounds in Table 1. The density functional calculations find a negative D value for the building block $[ReCl_4(CN)_2]^{2-}$ in all cases, no matter if the geometry is symmetrised or not or if counter-ions are included. This is in contrast to the experimental value for **1b** (Ref.[8]: ($D = +11$ cm^{-1}, $E = 3.2$ cm^{-1}) and a theoretical CASPT2 value for **1a** (Ref.[9]: $D = +16.2$ cm^{-1}, $E = 3.76$ cm^{-1}) which find a positive D and a very large rhombicity. Since density functional results can be quite sensitive to the choice of the exchange-correlation functional in general, and in particular to the amount of exact exchange included therein, we also tested how the calculated ZFS parameters depend on the amount of exact exchange. Varying the amount of exact exchange from 10% to 40% (the standard value for the PBE functional is 25%), the D value for **1a** varies from -32 to -24 and for **1b** from -34 to -26 cm^{-1} (see supporting information, Table S1 on page S9). It is therefore unlikely that the negative D value found in our DFT calculation is an artefact of the particular exchange-correlation functional chosen. The apparent discrepancy to experiment and CASPT2 calculations must have a more fundamental reason, and we will come back to this below. But an even more striking feature, found both in experiment and the CASPT2 calculations, is the large rhombicity $|E/D|$. This is striking because the building block is only slightly distorted from its ideal D_{4h} symmetry where $E = 0$.

Therefore we included symmetrised variants of **1a** in our investigation. The NC-Re-Cl angles in the X-ray structure of **1a** range from 88.6° to 91.4°, setting them to 90° but leaving all bond lengths unchanged gives a D_{2h} symmetric structure, replacing further the Re-Cl bond length by the average value of the two bond length found in the X-ray structure (234.1 and 235.1 pm) finally gives the D_{4h} symmetric variant. These are quite subtle geometry changes, and the calculated DFT energy slightly lowers when going from the X-ray structure to the D_{4h} variant (supporting information, Table S2 on page S38). We therefore assume that the deviation from the idealised

Table 1: ZFS parameters from density functional calculations for the mono- and trinuclear compounds. The second column lists the spin of the ground state. D and E values are given in cm^{-1}.

Cmpd.	remark	S	D	E
1a	D_{4h} variant	3/2	−26.98	0.00
	D_{2h} variant	3/2	−26.98	0.04
	X-ray structure	3/2	−26.95	0.74
1b	with counter-ions	3/2	−29.77	2.49
2		7/2	−3.06	0.11
3a	$\sim C_{2h}$	7/2	−2.83	0.15
3b	$\sim S_4$	7/2	−2.91	0.00

D_{4h} symmetry found in the X-ray structure is a crystal packing effect. The D_{4h} variant necessarily has $E = 0$ and this is found in the calculation (Table 1), but going then to the X-ray structure some rhombicity builds up, and it can be seen that E more strongly reacts to the variations in the NC-Re-Cl angles than to the differences in the Re-Cl bond lengths. The largest increase of the E value is however found when including the counter-ions (NBu_4^+). Still, the rhombicity found in the calculation is much smaller than found in the experiment, and this will be addressed in the next section.

For the trinuclear complexes **2** and **3a/b**, DFT also finds a negative D value of ~ 3 cm^{-1}. Within the strong exchange limit and assuming that the Mn^{II} ions contribute little to ZFS, one expects a molecular D value for the $S = 7/2$ ground state of the trinuclear complexes which is 1/15 (0.0667) of that of the Re^{IV} building block for which the same sort of calculation finds $D \sim -30$ cm^{-1}. Looking at the single-ion tensors (documented in the supporting information) which we have extracted from the DFT results and which were then used to calculate the molecular ZFS values, one sees that the Mn^{II} ions indeed do not contribute much to ZFS, which is consistent with their nearly spherical d^5 configuration. But coordinating the metals to the cyano ligands of the Re^{IV} core makes the local D value of the latter more negative, it goes from ~ -30 cm^{-1} (Table 1) to ~ -45 cm^{-1} (see the supporting information). Note that the experimental determination of the ZFS parameters for **2** [8] was difficult, but it seems clear that its experimental D value is rather small. Apparently the DFT calculations fail to predict the sign of D correctly, but the trend of making D more negative when coordinating metals to the cyano ligands of **1a** is compatible with the experiment, where one starts with a positive D value and moves towards zero upon coordinating the two Mn^{II}. As explained in the introduction, for a good SMM it is very important that the the ZFS tensor is uniaxial ($E \approx 0$), so it is a problem that we find a significant rhombicity for **2** ($|E/D| \approx 0.04$) which we first attributed to the fact that in the X-ray structure of **2**, the Re-CN-Mn linkages are bent which disturbs the local C_4 axis at the Re centre. This is why we constructed the hypothetical ligand $PyAm_4$ which supports, according to our geometry optimisations, linear linkages (see Sec. 2). For the S_4 symmetric conformation, we indeed find $E = 0$ (which is enforced

by symmetry), but rotating one of the end-caps by 90° (see Figure 2) is already enough to re-establish a significant value $E = 0.15$ cm^{-1}, which amounts to $|E/D| \approx 0.05$. To summarise, even if the negative sign of D found in the DFT calculations were correct, the large rhombicity built up even by small distortions suggests that **1a** is lacking the robustness that an ideal building block for SMMs should have.

3.2 CASOCI results

Heavy-element building blocks are being explored because spin-orbit coupling is strong there. $5d$ metal ions have spin-orbit coupling constants of a few thousand cm^{-1}, which is smaller, but not very much smaller, than the excitation energy to the lowest excited states. For $[ReCl_6]^{2-}$ for example, the lowest excited states are found slightly below 8000 cm^{-1} in spectroscopic experiments.[29,30] This leads to the question whether second-order spin-orbit perturbation theory, on which the DFT results in the preceding section are based, is still a valid method or whether higher-order spin-orbit effects can no longer be neglected. In principle, it is possible to go beyond perturbation theory with DFT, but this is numerically very delicate and it is difficult to get stable results. Therefore, we performed complete active space spin-orbit configuration interaction (CASOCI)[26] calculations where the spin-orbit interaction is included from the outset in the configuration interaction step. Although the orbitals to be used in CASOCI are still optimised in calculations without spin-orbit interaction, the CASOCI procedure includes the important higher-order spin-orbit effects. ZFS tensors and g values are then extracted from the CASOCI wave functions.[26] Spin-orbit coupling splits the quartet ground state of a Re^{IV} system into two pairs (Kramers doublets) of micro-states with an energy splitting of ~ 30 cm^{-1} (see Table 5). For each of the two Kramers doublets, the g values extracted from its two components are an independent measure of the rhombicity of the zero field splitting: in the uniaxial case ($E \approx 0$) one of the Kramers doublets has two g values close to zero ($g_1 \gg g_2 \approx g_3 \approx 0$), while for the other one the largest g occurs twice ($g_1 \approx g_2 > g_3$, assuming that we have sorted the g values such that $g_1 \geq g_2 \geq g_3$). The sign of D can also be deduces in this case: if $D < 0$, the lowest Kramers doublet is that one with two near-zero g values.

Table 2: CASOCI results for the ZFS for the mononuclear complexes. Besides the D and E parameters of the ground state quartet, the energy separation Δ of the two Kramers doublets and the g values for each of the two is given. D, E and Δ are in cm^{-1}.

Cmpd.	D	E	Δ	g values, lower doublet	g values, upper doublet
1a (D_{4h})	−14.75	0.00	29.5	5.40, 0.02, 0.02	3.66, 3.66, 1.75
1a (D_{2h})	−14.75	0.06	29.6	5.38, 0.33, 0.27	3.96, 3.35, 1.73
1a (X-ray)	−17.35	1.92	35.3	5.33, 0.64, 0.55	4.21, 3.04, 1.70
1b	−16.17	4.13	35.4	5.10, 1.44, 1.10	4.77. 2.23, 1.46

Table 2 contains the CASOCI results for the mononuclear compounds **1a** and **1b**. In all cases, a negative D value is found which comes to no surprise, since this was already reported for CASSCF-type wave functions in [9], there it was also demonstrated that it is necessary to add dynamical electron correlation to the wave function (Ref. [9] uses CASPT2) to arrive at a positive D value. Here we are mainly interested how strongly the rhombicity reacts to small perturbations. In agreement with the DFT results in the preceding section, we find that small changes in the Re-Cl bond lengths ($D_{4h} \rightarrow D_{2h}$) have little effect, while small changes in the NC-Re-Cl bond angles ($D_{4h} \rightarrow$ X-ray) give rise to a sizeable E value, and including the counter-ions (**1a** $\rightarrow$ **1b**) finally make ZFS extremely rhombic, with $|E/D| = 0.26$. This extreme rhombicity is more or less the same as found in the CASPT2 calculations ($|E/D| = 0.23$, [9]) and in experiment ($|E/D| = 0.29$, [8]) and much larger than the rhombicity found in our DFT calculations ($|E/D| = 0.08$, see Table 1). Note that the g values of the two Kramers doublets are fully consistent with the calculated $|E/D|$ ratios. They are given here for comparison with g values obtained from ligand field simulations (see next section). We note in passing that the increase of the rhombicity when going from **1a** to **1b** is largely induced by the electric field of the counter-ions, since similar results are obtained if one replaces the two NBu_4^+ cations by two Li^+ ions placed at the position of the (ammonium) nitrogen atoms. The main reason to discuss the CASOCI results is that we want to address why the DFT calculations strongly underestimated the build-up of rhombicity with increasing distortion of the ligand field. Our conjecture is that this happens because the DFT results are based on second-order spin-orbit perturbation theory while CASOCI also includes higher-order spin-orbit effects. This conjecture could be checked (and verified) with the following numerical experiment: in a series of CASOCI calculations, the spin-orbit interaction was scaled down with a parameter λ between 0 and 1, and the resulting D and E values then were up-scaled by multiplying with λ^{-2}.

Table 3: CASOCI ZFS parameters for the mononuclear complexes. In each line, the spin-orbit interaction has been multiplied by λ and the calculated D and E values (in cm^{-1}) have then be multiplied by λ^{-2}. This separates leading (second) order from higher-order spin-orbit effects.

	1a			**1b**		
λ	D	E	$\|E/D\|$	D	E	$\|E/D\|$
0.10	−18.40	1.25	0.07	−19.32	1.98	0.10
0.25	−18.53	1.33	0.07	−19.16	2.27	0.12
0.50	−18.49	1.50	0.08	−18.57	2.81	0.15
0.75	−18.10	1.69	0.09	−17.88	3.44	0.18
1.00	−17.35	1.92	0.11	−16.17	4.13	0.26

If higher-order spin-orbit effects were negligible, the D and E values (as well as the $|E/D|$ ratios) would be the same for all values of λ. But the results, presented in Table 3, clearly demonstrate that this is not the case. The second-order result is implicitly contained in the data by extrapolating to the limit $\lambda \rightarrow 0$, and it is clearly seen that the second-order result for $|E/D|$

is smaller than 0.10 even for compound **1b**. This means that the pronounced sensitivity of the ZFS rhombicity of the $[ReCl_4(CN)_2]^{2-}$ building block to small deviations of the ligand field is to a large part caused by higher-order spin-orbit effects. In our DFT calculations, which treat spin-orbit coupling by leading (second) order perturbation theory, these higher-order effects are missing and this explains why extreme rhombicity has not been obtained there.

3.3 Ligand field simulations

The CASOCI data (Table 2) indicates that when starting from the ideal uniaxial (D_{4h}) situation, different distortions of the ligand field produce very different amounts of rhombicity. This question, namely which distortions cause a large build-up of rhombicity, can be addressed more systematically by ligand field simulations. Ligand field simulations generally are a tool to analyse computational results rather than to make predictions, but in a well-defined context they can also be used to answer some ,,what if" questions. A ligand field model has been used to explore the zero field splitting of (distorted) $[ReF_6]^{2-}$ [31], where it was shown that tetragonal compression leads to a negative D. We extend this analysis to distortions with lower symmetry than tetragonal. The ligand field model is detailed in the supporting information. Since we keep the ratio of the Racah parameters C/B fixed, there is a single parameter (the Racah parameter B) to describe the electron interaction, a parameter Δ_{oct} describes the octahedral field, two parameters $\Delta^{\sigma}_{\mathrm{tet}}$ and $\Delta^{\pi}_{\mathrm{tet}}$ describe the σ and π contributions to the tetragonal distortion, and two parameters Δ_{rhomb} and Δ_{trig} are used to describe a rhombic and a trigonal distortion. The rhombic distortion makes the x and y axes inequivalent, while the trigonal distortion can be viewed as compressing the octahedron along one of its C_3 axes. The trigonal distortion has been included since the line joining the two NBu_4^+ cations in **1b** does not coincide with any of the C_4 axes of the octahedral environment of the Re^{IV} centre. The distortions are defined as parameters in a partial wave expansion of the ligand field in the supporting information, here we just remark that Δ_{oct} is the t_{2g}/e_g orbital energy splitting in the octahedral field, $\Delta^{\sigma}_{\mathrm{tet}}$ is the splitting of the e_g orbitals due to a tetragonal distortion ($\Delta^{\pi}_{\mathrm{tet}}$ the same for the t_{2g} orbitals).

First, we repeated a CASOCI calculation on **1a** in its D_{4h} variant but setting the spin-orbit interaction to zero. The resulting energy levels up to ~ 40000 cm^{-1} are given in Table 4, together with the energy levels of the ligand field model and a symmetry assignment, both for the actual D_{4h} symmetry of the molecule and the ,,parental" symmetry in the octahedral case. The tetragonal splitting of the low-energy $^2T(O_h)$ states is exclusively determined by $\Delta^{\pi}_{\mathrm{tet}}$ so this parameter has been fixed to reproduce the splitting of the (D_{4h}) $^2E_g/^2A_{2g}$ states that result from the (O_h) $^2T_{2g}$ state. Then, $\Delta^{\sigma}_{\mathrm{tet}}$ has been fixed to reproduce the splitting of the $^4T_{2g}$ state which depends on both tetragonal parameters. After this, Δ_{oct} has been fixed to reproduce the lowest excitation energy to the $^4T_{2g}$ manifold. The Racah parameter B as finally been adjusted to reproduce the excitation energy to the low-energy doublet states. The resulting values are $B = 652$ cm^{-1}, $\Delta_{\mathrm{oct}} = 35650$ cm^{-1}, $\Delta^{\sigma}_{\mathrm{tet}} = 6100$ cm^{-1} and $\Delta^{\pi}_{\mathrm{tet}} = -2400$ cm^{-1}. These parameters come from adjusting energy levels but make much sense: $\Delta^{\sigma}_{\mathrm{tet}}$ is large and positive which reflects that the cyano ligand is a much stronger σ donor than chloride. On the other hand, $\Delta^{\pi}_{\mathrm{tet}}$ is negative because chlorido ligands are π donors while cyano ligands are π acceptors. The B value seems to be rather high, compared

Table 4: Ab initio (CASOCI) and ligand field simulation energies (in cm^{-1} relative to the ground state) for **1a** (D_{4h} variant), **without** spin-orbit interaction. The ligand field parameters (see the supporting information for their definition) are B = 652 cm^{-1}, Δ_{oct} = 35650 cm^{-1}, Δ^{σ}_{tet} = 6100 cm^{-1}, Δ^{π}_{tet} = −2400 cm^{-1}. The symmetry assignment (third column) comes from an analysis of the wave functions from the ligand field simulation, and the second column lists the ,,parental" symmetry for the perfect octahedral case. The symmetry assignment of lowest CASOCI excited states (below 13500 cm^{-1}) is tentative but suggested by the splitting pattern.

CASOCI Energy	Sym O_h	Sym D_{4h}	Simulation Energy
0	$^4A_{2g}$	$^4B_{1g}$	0
13179	$^2T_{1g}$	^2E_g	13251
13219	^2E_g	$^2B_{1g}$	13479
13304	^2E_g	$^2A_{1g}$	13502
13891	$^2T_{1g}$	$^2A_{2g}$	13921
21604	$^2T_{2g}$	$^2B_{2g}$	21608
22308	$^2T_{2g}$	^2E_g	22299
30982	$^4T_{2g}$	$^4B_{2g}$	31000
36767	$^4T_{2g}$	^4E_g	36728

to B = 443 cm^{-1} reported by Jørgensen for $[ReCl_6]^{2-}$ [29]. This corresponds to an over-estimation of the excitation energy to the low-energy doublets in CASOCI, which is indeed the case and can only be corrected by including dynamical correlation. At this point we did a perturbational estimate of the spin-orbit induced mixing of the excited states with the ground state quartet and found that they contribute to the D value with opposite sign. In the leading order of spin-orbit perturbation theory, these contributions are inverse proportional to the excitation energy, therefore it becomes clear why including dynamical electron correlation (which mainly affects the excitation energy to the low-energy doublets but not to the lowest quartet) boosts the contribution from the low-energy doublets and has such a strong effect on the sign of D.

To complete the ligand field model, we have to adjust the value of the spin-orbit coupling constant. For this, the above ligand field parameters have been kept fixed and the spin-orbit coupling constant chosen to reproduce the CASOCI energy levels including spin-orbit interaction. We decided to reproduce the splitting of the $^2T_{2g}$ manifold, and this resulted in a spin-orbit coupling constant ζ_{SO} = 2700 cm^{-1}. This value is larger than the value reported by Jørgensen for $[ReCl_6]^{2-}$ [29], but the spin-orbit coupling constant there had quite come uncertainty (2400 ± 480 cm^{-1}) and our value is within this range. The results from our ligand field simulation with

Table 5: Ab initio (CASOCI) and ligand field simulation energies (in cm^{-1} relative to the ground state) for **1a** (D_{4h} variant), **with** spin-orbit interaction. The ligand field parameters are the same as in Table 4 except that now we have a spin-orbit coupling constant ζ_{SO} = 2700 cm^{-1}. All listed energy levels are Kramers doublets. The symmetry label (column 2) is the ,,parental" symmetry of the states in perfect octahedral symmetry without spin-orbit coupling. Note that spin-orbit coupling mixes E_g and T_{1g} octahedral states.

CASOCI Energy	Sym O_h	Simulation Energy
0	$^4A_{2g}$	0
29		11
11779	$^2E_g/^2T_{1g}$	11916
12807		13035
13474		13534
13820		13848
14296		14374
22587	$^2T_{2g}$	22544
23170		22952
24496		24342
31441	$^4T_{2g}$	31438
31805		31777
36007		36293
37485		37421
38084		37724
38677		37967

spin orbit coupling, compared to the CASOCI energy levels, are shown in Table 5. The limit of the ligand-field model becomes obvious. Although the low-lying excitation energies are well reproduced, the zero field splitting of the ground state quartet from the ligand field model is much smaller (11 cm^{-1}, $D = -5.5$ cm^{-1}) than for CASOCI (29 cm^{-1}, $D = -14.8$ cm^{-1}). The excitation energy to the lowest spin-orbit coupled doublet state is slightly below 12000 cm^{-1} and thus much higher than the lowest excitation energy observed experimentally for $[ReCl_6]^{2-}$ [29,30]. This is consistent with the fact that our B parameter (652 cm^{-1}, adjusted to reproduce CASOCI data) is significantly higher than the B value (443 cm^{-1}) adjusted to fit experimental data for $[ReCl_6]^{2-}$ [29]. The ligand model is nevertheless useful. For example, the sensitivity of the resulting D value to the computational method becomes clear: axial compression leads to a negative D, as

already shown within the ligand field model in Ref.[31]. But here we have axial compression in $V_{\rm tet}^{\sigma}$ but axial expansion in $V_{\rm tet}^{\pi}$, so there are contributions with different sign. Even more, since the low-lying doublets from the t_{2g}^3 manifold are only affected by $V_{\rm tet}^{\pi}$, lowering their energy will increase the positive contributions to D. This means that CASOCI will probably underestimate the contribution of the low-energy doublets to zero field splitting and that including dynamical correlation (such as in the CASPT2 calculations of Ref.[9]) has a substantial effect on calculated ZFS parameters. This can also be extracted from ligand field simulations: Reducing the Racah B parameter from 652 to 443 cm^{-1}, we also find a positive D value in the ligand field simulations: the splitting between the lowest Kramers doublets increases from 11 to 21 cm^{-1} but the order of the Kramers doublets is reversed, the one with $g_2 \approx g_3 \approx 0$ now is the higher one, such hat we have $D = +10.5$ cm^{-1} here. In the ligand field simulation, this reduction of the B parameter reduces the excitation energy to the lowest doublet from ~ 12000 to ~ 7500 cm^{-1}. This is useful information since the change of sign of D occurs here for a case where $E = 0$, where the sign of D is well defined. In contrast, both in the experiment[8] and in the CASPT2 calculations[9], there was a very large rhombicity and the sign of D looses its meaning when $|E/D|$ approaches 0.33 which is its theoretical limit.

Table 6: g values for the lower and upper Kramers doubled arising from the ZFS of the quartet ground state from ligand field simulations, for the idealised D_{4h} case and after applying various perturbations to the ligand field. In the first line, ligand-field parameters are the same as in Table 5 and in subsequent lines a rhombic or trigonal distortion has been applied on top of that. $\Delta_{\rm rhomb}$ and $\Delta_{\rm trig}$ are given in cm^{-1}.

$\Delta_{\rm rhomb}$	$\Delta_{\rm trig}$	g values, lower doublet	g values, upper doublet
0	0	5.15, 0.04, 0.04	3.52, 3.52, 1.64
$\pm$200	0	5.09, 0.62, 0.49	4.05, 2.94, 1.58
0	$-$200	5.02, 0.86, 0.79	4.28, 2.60, 1.55
0	+200	4.82, 1.43, 1.16	4.63, 2.06, 1.33

Now we are in a position to discuss the effect of the distortions of the ligand field on the ZFS rhombicity of the ground state quartet. To this end, the g values of the two lowest Kramers doublets of the wave functions of the ligand field simulation have been calculated for the model just presented (using our original B value of 652 cm^{-1}). We did this for the uniaxial case and for cases where one additionally applies a rhombic or trigonal distortion (Table 6). We have applied rather small distortions (200 cm^{-1}), this value directly corresponds to orbital energy splittings induced by the perturbation. We see that a rhombic distortion ($D_{4h} \rightarrow C_{2h}$) only builds up a small rhombicity. The sign of the distortion does not matter since it only indicates if the stronger ligand field is in the x or y direction. For a trigonal distortion, the effect on the rhombicity is much larger. Note that in the experimental structure of $(NBu_4)_2ReCl_4(CN)_2$,[7] the counter-ions are placed on a line that roughly bi-sects a Cl-Re-CN angle, and therefore induce a perturbation

similar to such a trigonal one. This helps explaining why including the counter-ions when going from **1a** to **1b** (see Tables 1,2) has such a large impact on the calculated rhombicity. For **1b**, it thus seems that the counter-ions induce the largest part of the rhombicity observed experimentally, [8] and that the small geometrical distortions of the $[ReCl_4(CN)_2]^{2-}$ unit are of lesser importance.

4 Conclusions

Putting everything together, one can say that building blocks with $5d$ centres behave different from hypothetical $3d$ centres with increased zero field splitting. The ligand field is stronger for the $5d$ elements due to increased covalency, but the atomic exchange integrals are smaller because the electrons in the $5d$ orbitals have a larger mean distance from each other compared to the more compact $3d$ orbitals. This means that the relative importance of ligand-field excited states with the same spin on one hand, and spin-flip excited states without $t_{2g} \rightarrow e_g$ promotion on the other hand, is very different: in a $5d$ ion with octahedral t_{2g}^3 quartet configuration for example, the doublets from the t_{2g}^3 manifold are much lower than the ligand-field excited $(t_{2g}^2 e_g^1)$ quartets, but in an analogous $3d$ compound, this is not the case. This is the reason why the exact energetic position of the lowest doublets is much more important in $5d$ than in $3d$ compounds. Furthermore, for $5d$ compounds the excitation energy to the low-lying doublets is no longer small compared to the spin-orbit coupling constant, which limits the liability of leading-order spin-orbit perturbation theory and one has to include higher orders, which is difficult to do (at least if high numerical accuracy is wanted) within the DFT framework. So although using octahedral Re^{IV} centres as ,,spin-orbit boosters" for SMMs looks promising at first sight, a closer analysis shows that there are also problems associated with this type of spin centre that might be difficult to overcome.

Acknowledgements

his work has been funded by Deutsche Forschungsgemeinschaft through the collaborative research center SfB/TRR 88 ,,3Met". Computer time was provided by AHRP, the state alliance for high performance computing, on the university computer ,,Elwetritsch" of the Technische Universität Kaiserslautern.

Abbreviations

The following abbreviations are used in this manuscript:

CASOCI	complete active space valence configuration interaction with spin-orbit coupling
CASPT2	complete active space with second-order perturbation theory
CASSCF	complete active space self-consistent field
DEA	diethyl formamide
DFT	density functional theory
DMF	dimethyl formamide
EPR	electron paramagnetic resonance
SMM	single molecule magnet
ZFS	zero field splitting

Supporting Information

Electronic supporting information for this article is available (PDF file, 39 pages). It documents the extraction of single-ion spin Hamiltonian parameters (Sec. S1), the dependence of the calculated zero field splitting parameters for compounds **1a,b** on the amount of exact exchange in the exchange-correlation functional (Sec. S2), it gives details to the ligand field simulation model (Sec. S3), and finally documents the cartesian (XYZ) coordinates (Sec. S4) and DFT total energies (Sec. S5) of all compounds.

References

[1] M. Affronte, *J. Mater. Chem.* **2009**, *19*, 1731–1737.

[2] F. Troiani, M. Affronte, *Chem. Soc. Rev.* **2011**, *40*, 3119–3129.

[3] D. Gatteschi, R. Sessoli, J. Villain, *Molecular Nanomagnets*, Oxford University Press, New York, **2006**.

[4] X. Y. Wang, C. Avendano, K. R. Dunbar, *Chem. Soc. Rev.* **2011**, *40*, 3213–3238.

[5] M. V. Bennett, J. R. Long, *J. Am. Chem. Soc.* **2003**, *125*, 2394–2395.

[6] J. M. Zadrozny, D. E. Freedman, D. M. Jenkins, T. D. Harris, A. T. Iavarone, C. Mathoniere, R. Clerac, J. R. Long, *Inorg. Chem.* **2010**, *49*, 8886–8896.

[7] T. D. Harris, M. V. Bennett, R. Clerac, J. R. Long, *J. Am. Chem. Soc.* **2010**, *132*, 3980–3988.

[8] X. W. Feng, J. J. Liu, T. D. Harris, S. Hill, J. R. Long, *J. Am. Chem. Soc.* **2012**, *134*, 7521–7529.

[9] S. K. Singh, G. Rajaraman, *Nat. Commun.* **2016**, *7*, 10669.

[10] S. K. Singh, K. R. Vignesh, V. Archana, G. Rajaraman, *Dalton Trans.* **2016**, *45*, 8201–8214.

[11] C. Adamo, V. Barone, *J. Chem. Phys.* **1999**, *110*, 6158.

[12] F. Weigend, R. Ahlrichs, *Phys. Chem. Chem. Phys.* **2005**, *7*, 3297.

[13] D. Andrae, U. Häussermann, M. Dolg, H. Stoll, H. Preuss, *Theor. Chim. Acta* **1990**, *77*, 123–141.

[14] R. Ahlrichs, M. Bär, M. Häser, H. Horn, C. Kölmel, *Chem. Phys. Lett.* **1989**, *162*, 165.

[15] M. Häser, R. Ahlrichs, *J. Comput. Chem.* **1989**, *10*, 104.

[16] C. van Wüllen, *Chem. Phys. Lett.* **1994**, *219*, 8.

[17] C. Peng, P. Ayala, H. B. Schlegel, M. J. Frisch, *J. Comput. Chem.* **1996**, *17*, 49.

[18] M. J. Frisch, G. W. Trucks, H. B. Schlegel, G. E. Scuseria, M. A. Robb, J. R. Cheeseman, G. Scalmani, V. Barone, G. A. Petersson, H. Nakatsuji, X. Li, M. Caricato, A. V. Marenich, J. Bloino, B. G. Janesko, R. Gomperts, B. Mennucci, H. P. Hratchian, J. V. Ortiz, A. F. Izmaylov, J. L. Sonnenberg, D. Williams-Young, F. Ding, F. Lipparini, F. Egidi, J. Goings, B. Peng, A. Petrone, T. Henderson, D. Ranasinghe, V. G. Zakrzewski, J. Gao, N. Rega, G. Zheng, W. Liang, M. Hada, M. Ehara, K. Toyota, R. Fukuda, J. Hasegawa, M. Ishida, T. Nakajima, Y. Honda, O. Kitao, H. Nakai, T. Vreven, K. Throssell, J. A. Montgomery, Jr., J. E. Peralta, F. Ogliaro, M. J. Bearpark, J. J. Heyd, E. N. Brothers, K. N. Kudin, V. N. Staroverov, T. A. Keith, R. Kobayashi, J. Normand, K. Raghavachari, A. P. Rendell, J. C. Burant, S. S. Iyengar, J. Tomasi, M. Cossi, J. M. Millam, M. Klene, C. Adamo, R. Cammi, J. W. Ochterski, R. L. Martin, K. Morokuma, O. Farkas, J. B. Foresman, D. J. Fox, *Gaussian 16, Revision A.03*, Gaussian, Inc., Wallingford, CT, 2016.

[19] X. W. Feng, T. D. Harris, J. R. Long, *Chem. Sci.* **2011**, *2*, 1688–1694.

[20] M. Reiher, *WIREs Comp. Mol. Sci* **2012**, *2*, 139–149.

[21] C. van Wüllen, C. Michauk, *J. Chem. Phys.* **2005**, *123*, 204113.

[22] F. Neese, *J. Chem. Phys.* **2005**, *122*, 034107.

[23] S. Schmitt, P. Jost, C. van Wüllen, *J. Chem. Phys.* **2011**, *134*, 194113.

[24] E. M. V. Kessler, S. Schmitt, C. van Wüllen, *J. Chem. Phys.* **2013**, *139*, 184110.

[25] T. Nakajima, K. Hirao, *J. Chem. Phys.* **2002**, *116*, 8270–8275.

[26] T. Bodenstein, A. Heimermann, K. Fink, C. van Wüllen, *ChemPhysChem* **2022**, in press, doi.org/10.1002/cphc.202100648.

[27] B. A. Hess, C. M. Marian, U. Wahlgren, O. Gropen, *Chem. Phys. Lett.* **1996**, *251*, 365–71.

[28] A. Heimermann, C. van Wüllen, *Chem. Eur. J* **2021**, *27*, 15148–15158.

[29] C. K. Jørgensen, K. Schwochau, *Z. Naturforsch. A* **1965**, *20*, 65–75.

[30] J. C. Eisenstein, *J. Chem. Phys.* **1961**, *34*, 1628–1648.

[31] K. S. Pedersen, M. Sigrist, M. A. Sørensen, A.-L. Barra, T. Weyhermüller, S. Piligkos, C. A. Thuesen, M. G. Vinum, H. Mutka, H. Weihe, R. Clerac, J. Bendix, *Angew. Chem.-Int. Edit.* **2014**, *53*, 1351–1354.